AGU PUBLICATIONS

Water Resources Research

RESEARCH ARTICLE
10.1002/2016WR019263

Use and misuse of large-density asymptotics in the reaction-infiltration instability

Anthony J. C. Ladd[1] **and Piotr Szymczak**[2]

[1]Department of Chemical Engineering, University of Florida, Gainesville, Florida, USA, [2]Institute of Theoretical Physics, Faculty of Physics, University of Warsaw, Warsaw, Poland

Key Points:
- A critique of the literature relating to the reaction-infiltration instability in porous materials is presented
- A large ratio of mineral to reactant concentrations does not imply that the dissolution front is sharp
- The thickness of a dissolution front in reaction-infiltration is controlled by the flow rate, reaction rate and reactant diffusivity

Correspondence to:
A. J. C. Ladd,
tladd@che.ufl.edu

Citation:
Ladd, A. J. C. and P. Szymczak (2017), Use and misuse of large-density asymptotics in the reaction-infiltration instability, *Water Resour. Res.*, *53*, doi:10.1002/2016WR019263.

Received 24 MAY 2016
Accepted 19 FEB 2017
Accepted article online 23 FEB 2017

Abstract Analyzing the dissolution of rocks and other porous materials is simplified by the large disparity between mineral and reactant concentrations. In essence, the porosity remains frozen on the time scale of the reactant transport, which can then be treated as a quasi-stationary process. This conceptual idea can be derived mathematically using asymptotic methods, which show that the length scales in the system are, to a first approximation, independent of the ratio of reactant and mineral concentrations. Nevertheless, in a growing number of papers on dissolutional instabilities, the reactant-mineral concentration ratio has been incorrectly linked to the thickness of the dissolution front. In this paper we critically review the application of asymptotic methods to the reaction-infiltration instability. In particular, we discuss the limited validity of the thin-front or "Stefan" limit, where the interface between dissolved and undissolved mineral is sharp.

1. Introduction

When an acidic solution is injected into a soluble porous matrix, for example, calcite or gypsum, the dissolution front does not necessarily remain planar. One important consequence is that the permeability increase during reservoir acidization depends nonmonotonically on flow rate [*Rowan*, 1959], with the maximum corresponding to the spontaneous development of highly localized flow paths, or "wormholes." Wormhole formation has been investigated in the laboratory using a variety of materials: plaster (gypsum) dissolved by water [*Ewers*, 1982; *Daccord*, 1987; *Osselin et al*., 2016], acidized limestone cores [*Hoefner and Fogler*, 1988; *Fredd and Fogler*, 1998; *Polak et al*., 2004; *Luquot and Gouze*, 2009; *Noiriel et al*., 2013; *Luquot et al*., 2014], KH_2PO_4 crystals [*Detwiler et al*., 2003; *Detwiler*, 2010], and salt [*Kelemen et al*., 1995; *Golfier et al*., 2002].

In a seminal paper, *Chadam et al*. [1986] proposed a simple feedback mechanism to explain the instability of a dissolution front. A region of slightly enhanced porosity draws flow and reactant from the surrounding regions, and therefore dissolves more quickly. This in turn increases the flow to that region, amplifying the porosity contrast with the neighboring material. A linear stability analysis was used to estimate the wavelengths of unstable perturbations in the front position. They found both a simple criterion for an unstable front, and a formula for the growth rate and wavelength of the most unstable mode. Subsequently, in two influential papers [*Ortoleva et al*., 1987a, 1987b], they reframed their insights within a geological context. However, their papers [*Chadam et al*., 1986; *Ortoleva et al*., 1987b; *Chadam et al*., 1988, 2001] also contain a crucial misconception, which they refer to as "large solid-density asymptotics." They deduced (incorrectly) that a large ratio of mineral to aqueous concentrations inevitably means that the interface between the dissolved and undissolved mineral is sharp.

It has been pointed out several times, beginning with *Hinch and Bhatt* [1990] and *Steefel and Lasaga* [1990], that the analysis in *Chadam et al*. [1986] is only valid in the fast-reaction limit [*Wangen*, 2013; *Szymczak and Ladd*, 2014]. Nevertheless, the erroneous connection between mineral-reactant concentration ratio and the thickness of the porosity front persists to the present day [*Zhao et al*., 2008, 2010, 2013a; *Zhao*, 2014; *Zhao et al*., 2014, 2015; *Lai et al*., 2016]. In this paper we retrace the original derivation from *Chadam et al*. [1986], pointing out that they are, in effect, taking two limits simultaneously. One is the limit they discuss, namely that the solution concentration is much smaller than the mineral concentration. But there is also a hidden assumption of fast-reactions, which makes for the discontinuous change in porosity [*Lichtner*, 1988; *Phillips*,

Table 1. Symbols Used in the Paper, Grouped by Fields, Input Parameters, and Derived Scales[a]

Fields		Input Parameters		Derived Scales	
ϕ	Porosity	s	Specific surface area	l_p	penetration length (11)
$\mathbf{v}$	Velocity	v_0	Outlet velocity	U	front velocity (43)
c	Concentration	c_{in}	Inlet concentration	t_r	reaction time scale (19)
$K(\phi)$	Permeability	k	Reaction rate constant	t_d	dissolution time scale (20)
		D	Diffusion coefficient	H	transport parameter (25)
		c_{sol}	Mineral concentration	γ	dissolution ratio (8)
				Γ	permeability ratio K_0/K_1

[a]Subscripts 0 and 1 in the text refer to the undissolved and fully dissolved matrix; for example $K_0=K(\phi_0)$ refers to the permeability and porosity of the undissolved matrix.

1990; *Steefel and Lasaga*, 1990]. We also introduce a more general analysis [*Szymczak and Ladd*, 2014], which allows for finite reaction rates and a gradual transition in porosity across the front. The symbols used in the paper are summarized in Table 1.

2. Fundamental Equations and Scales

Dissolution of a porous matrix involves the interplay of transport processes, convection, and dispersion, with chemical reactions at the solid surfaces. Since reaction rates and flow velocities in subsurface transport can vary by many orders of magnitude, different regimes of dissolution are possible. To elucidate the possibilities, we begin with the equations for reactive transport in porous media [*Chadam et al.*, 1986; *Steefel and Lasaga*, 1990; *Golfier et al.*, 2002], which are balance equations for the mass of (incompressible) solvent, reactant, and mineral

$$\partial_t\phi+\nabla\cdot\boldsymbol{v}=0, \tag{1}$$

$$\partial_t(\phi c)+\nabla\cdot(\boldsymbol{v}c)=\nabla\cdot\boldsymbol{D}\cdot\nabla c-R(c,\phi), \tag{2}$$

$$c_{sol}\partial_t\phi=R(c,\phi). \tag{3}$$

In these equations ϕ is the matrix porosity, $\boldsymbol{v}$ is the superficial or Darcy velocity, c is the reactant concentration field, and c_{sol} is the concentration of consolidated mineral. The Darcy velocity is related to the mean fluid velocity in the pore space ($\boldsymbol{u}$) by $\boldsymbol{v}=\phi\boldsymbol{u}$, with $\nabla\cdot\boldsymbol{u}=0$.

We will assume that the rock contains some insoluble material, so that Darcy's law can be used to represent the fluid momentum balance even as the rock dissolves,

$$\boldsymbol{v}=-\frac{K}{\mu}\nabla p, \tag{4}$$

where $K(\phi)$ is the permeability, p is the pressure, and μ is the fluid viscosity. Because the qualitative features of the reaction-infiltration instability are insensitive to the precise form of the constitutive models [*Szymczak and Ladd*, 2014], we use a minimal reactive transport model; namely, a constant isotropic dispersion, $\boldsymbol{D}=D\mathbf{1}$, and a linear reaction rate,

$$R(c,\phi)=kcs\,\Theta(\phi_1-\phi), \tag{5}$$

with a constant specific surface area s. The Heaviside function,

$$\Theta(x)=0 \quad x\le 0, \tag{6}$$

$$\Theta(x)=1 \quad x>0, \tag{7}$$

limits the reaction to partially dissolved regions where the porosity is less than its maximum value ϕ_1. A dissolution reaction can also be described in terms of the undersaturation of aqueous mineral ions $R=k(c_{sat}-c)s$ [*Plummer and Wigley*, 1976]. Equation (2) is then replaced by an identical equation for the undersaturation $C=c_{sat}-c$; the subsequent analysis follows section 3 with the exception that C is scaled by c_{sat} rather than the inlet concentration c_{in}.

In geological settings, there is usually a large difference between the reactant concentration in the incoming fluid stream c_{in} and the mineral concentration c_{sol}. The ratio of these two concentrations,

$$\gamma=\frac{c_{in}}{c_{sol}}, \tag{8}$$

is then a small parameter; for example, in the dissolution of natural calcite γ is of the order of 10^{-4}. Physically, this means that on time scales where the flow and reactant transport come to a quasi-

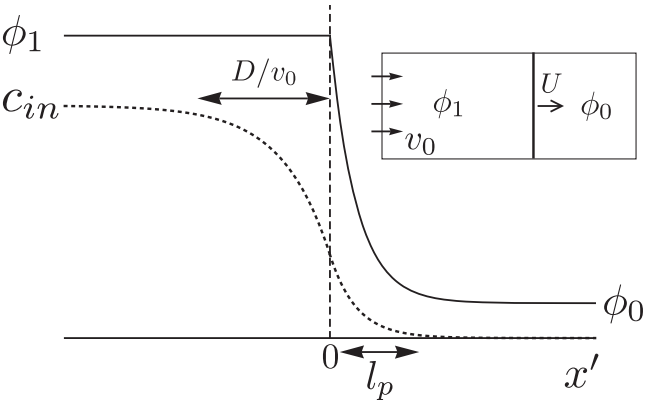

Figure 1. Concentration and porosity profiles for a planar front; the position of the front in the moving coordinate system $x'=x-Ut$ is indicated by the dashed vertical line. The concentration, c (dotted line), decays with different length scales, D/v_0 and l_p, in the upstream ($x'<0$) and downstream ($x'>0$) regions.

stationary state, the porosity remains unchanged. Thus, it will be possible to drop the time derivatives in equations (1) and (2), but not in (3) where the evolution is much slower. These qualitative considerations will be substantiated with mathematical analysis in section 3.

As an initial condition we can imagine a sharp planar boundary between dissolved and undissolved mineral, located at $x=0$. Upstream of the front ($x<0$) the mineral is fully dissolved while downstream of the front ($x>0$) it is entirely undissolved. Reactant is introduced far upstream at constant velocity v_0 with concentration c_0. Downstream of the front the reactant concentration eventually vanishes, while the flow velocity returns to a uniform value v_0.

The front broadens and propagates over time, eventually reaching a steady state in a frame $x'=x-Ut$ moving with a fixed velocity U. The concentration profile is illustrated schematically in Figure 1. The dissolution front (dashed line) advances into the undissolved matrix (porosity ϕ_0); to the left of the front (porosity ϕ_1) all the soluble material has dissolved, whereas to the right of the front there is a region of partially dissolved material.

The stationary concentration field is given by [*Szymczak and Ladd*, 2013]

$$\frac{c}{c_{in}}=1-\frac{e^{v_0x'/D}}{1+v_0l_p/D} \quad x'<0, \tag{9}$$

$$\frac{c}{c_{in}}=\frac{e^{-x'/l_p}}{1+D/v_0l_p} \quad x'>0, \tag{10}$$

where both the concentration (c) and the flux (v_0c-Ddc/dx') are continuous at the interface ($x'=0$). Upstream of the front ($x'<0$ in Figure 1) the porosity is constant and all reaction has ceased; the concentration near the front decays with a length scale D/v_0 (9). The thickness of the porosity front ($x'>0$) is given by the reactant penetration length [*Lichtner*, 1988; *Phillips*, 1990; *Steefel and Lasaga*, 1990],

$$l_p=\frac{2D}{(v_0^2+4Dks)^{1/2}-v_0}, \tag{11}$$

where v_0 is the velocity of the incoming fluid. In subsurface rocks l_p ranges from less than 1 mm to 100 m [*Phillips*, 1990; *Szymczak and Ladd*, 2013].

Two important limiting cases can be identified from the one-dimensional concentration profile given by equations (9) and (10). When the downstream length dominates, $l_p \gg D/v_0$, the concentration profile appears constant right up to the front, decaying exponentially (for linear reaction kinetics) into the porous matrix

$$c=c_{in} \quad x<0, \tag{12}$$

$$c=c_{in}e^{-x/l_p} \quad x>0. \tag{13}$$

On the other hand, when the upstream length is dominant, $l_p \ll D/v_0$; now the concentration does not penetrate into the matrix, but is entirely consumed in a thin region at the front

$$c=c_{in}\left(1-e^{v_0x/D}\right) \quad x<0, \tag{14}$$

$$c=0 \quad x>0. \tag{15}$$

Equations (12)–(15) summarize (for a planar front) the two key limiting cases of the reaction-infiltration instability. In the first case, (12) and (13), dispersion is negligible and the penetration into the matrix is set by the balance between convection and reaction $l_p=v_0/ks$. This is typically the case for fracture dissolution [*Szymczak and Ladd*, 2012], but it can also occur in porous materials when the reaction rates are slow [*Phillips*, 1990; *Szymczak and Ladd*, 2013]. In the second case, (14) and (15), the reaction rate is large and the infiltrating solution is always in a condition of local equilibrium [*Lichtner*, 1988; *Steefel and Lasaga*, 1990]. Here the reactant does not penetrate into the matrix and only the upstream length is significant, set by the balance of dispersion and convection. Thus, the thickness of the porosity front is determined by transport parameters (D, v_0, and ks) and not by γ, as suggested in a number of publications [*Chadam et al*., 1986; *Ortoleva et al*., 1987a; *Chadam et al*., 1988; *Chadam and Ortoleva*, 1990; *Chadam et al*., 2001; *Zhao et al*., 2008, 2013a, 2013b; *Zhao*, 2014; *Zhao et al*., 2014].

3. Asymptotic Limits

If the initial front is not exactly planar then a variety of evolving interface shapes become possible, due to the instability mechanism first described by *Chadam et al*. [1986]. In this section we discuss a more general approach to the instability problem [*Szymczak and Ladd*, 2013] and point out its connection to the earlier theory [*Chadam et al*., 1986].

We have already noted that there are two natural length scales that arise in the transport equations (9 and 10): the upstream length D/v_0 and the downstream penetration length l_p (11). Here we scale distance by the upstream length,

$$\tilde{\boldsymbol{r}}=\frac{\boldsymbol{r}v_0}{D}, \tag{16}$$

which ensures that the distance scale remains finite in the fast-reaction limit ($l_p \ll D/v_0$). In addition to the distance scaling, $\boldsymbol{v}$ is scaled by the flow velocity in a uniform (undissolved) matrix v_0 and c is scaled by the inlet concentration c_{in}

$$\tilde{\boldsymbol{v}}=\frac{\boldsymbol{v}}{v_0}, \quad \tilde{c}=\frac{c}{c_{in}}. \tag{17}$$

The permeability of the undissolved matrix $K_0=K(\phi_0)$ and $v_0=-K_0\nabla p/\mu$. The dimensionless version of Darcy's law is then

$$\tilde{\boldsymbol{v}}=-\tilde{K}\tilde{\nabla}\tilde{p}, \tag{18}$$

where $\tilde{K}=K/K_0$ and $\tilde{p}=pK_0/\mu D$.

When a reactive fluid comes in contact with soluble mineral, reactant is consumed on a time scale

$$t_r=\frac{1}{ks}, \tag{19}$$

while mineral dissolution is characterized by a slower time scale,

$$t_d=\frac{t_r}{\gamma}=\frac{1}{ks\gamma}. \tag{20}$$

We nondimensionalize the time with t_d,

$$\tilde{t}=\frac{t}{t_d}=ks\gamma t, \tag{21}$$

so that an order one variation in ϕ requires a dimensionless time $\tilde{t}\sim 1$. With the scalings from (16), (17), and (21), equations (1)–(3) are

$$\gamma H\tilde{\partial}_t\phi+\tilde{\nabla}\cdot\tilde{\boldsymbol{v}}=0, \tag{22}$$

$$\gamma H\tilde{\partial}_t(\phi\tilde{c})+\tilde{\nabla}\cdot(\tilde{\boldsymbol{v}}\tilde{c})=\tilde{\nabla}^2\tilde{c}-H\tilde{c}\,\Theta(\phi_1-\phi), \tag{23}$$

$$\tilde{\partial}_t\phi=\tilde{c}\,\Theta(\phi_1-\phi). \tag{24}$$

The dimensionless group H, given by

$$H=\frac{Dks}{v_0^2}, \tag{25}$$

can vary widely: combining natural systems, acidization, and laboratory experiments, H spans a range from $10^{-4} < H < 10^3$ [*Szymczak and Ladd*, 2013].

The dimensionless equations (22)–(24) contain two independent parameters, γ and H. However, the large ratio of mineral to reactant concentration, $\gamma \ll 1$, implies that the time derivative in equations (22) and (23) can usually be neglected; the flow and concentration fields are in a quasi-steady state, slaved to the slowly evolving porosity field. If we take the position of the front $x_f(y)$ as the boundary between fully ($\phi=\phi_1$) and partially ($\phi < \phi_1$) dissolved mineral, then in the upstream region, $x < x_f$

$$\tilde{\nabla}\cdot\tilde{\boldsymbol{v}}=0, \tag{26}$$

$$\tilde{\nabla}\cdot(\tilde{\boldsymbol{v}}\tilde{c})=\tilde{\nabla}^2\tilde{c}, \tag{27}$$

$$\tilde{\phi}=\phi_1. \tag{28}$$

Downstream of the front, $x > x_f$,

$$\tilde{\nabla}\cdot\tilde{\boldsymbol{v}}=0, \tag{29}$$

$$\tilde{\nabla}\cdot(\tilde{\boldsymbol{v}}\tilde{c})=\tilde{\nabla}^2\tilde{c}-H\tilde{c}, \tag{30}$$

$$\tilde{\partial}_t\phi=\tilde{c}. \tag{31}$$

The velocity and concentration fields are now explicit functions of position only, while H is the sole parameter characterizing the dimensionless equations.

Although the interface dividing dissolved and undissolved minerals is not always sharp [*Lichtner*, 1988], the thin-front limit, meaning $D/v_0 \gg l_p$ or $H \gg 1$, occurs frequently in nature and sometimes in reservoir acidization as well [*Szymczak and Ladd*, 2013]. Taking $H \to \infty$ in equation (30) implies that $\tilde{c}$ must vanish in the downstream region

$$\tilde{\nabla}\cdot\tilde{\boldsymbol{v}}=0, \tag{32}$$

$$\tilde{c}=0, \tag{33}$$

$$\tilde{\phi}=\phi_0. \tag{34}$$

More precisely, as $H \to \infty$ the gradients of $\tilde{c}$ in equation (30) must become ever steeper in order to balance the term $H\tilde{c}$. The penetration length into the matrix $l_p \to \sqrt{D/ks}$ becomes vanishingly small in comparison to the concentration length scale in the upstream region D/v_0. The quasi-stationary thin-front limit described by *Chadam et al.* [1986] therefore involves two sequential limiting steps: first $\gamma \to 0$ (29)–(31), then $H \to \infty$ (32)–(34); we return to this point in the next section.

By invoking a quasi steady state in equations (26)–(31), we have implicitly assumed that the dissolution time scale is the longest in the system, $t_d \gg \max(t_r, D/v_0^2)$ (Appendix A). This imposes two different conditions on the validity of equations (27) and (30), depending on the value of H. For $H < 1$ ($t_r > D/v_0^2$), the condition for a quasi-steady state is $t_d \gg t_r$, or

$$.\gamma \ll 1. \tag{35}$$

On the other hand, when $H > 1$ (and $D/v_0^2 > t_r$) the quasi steady state condition is $t_d \gg D/v_0^2$, or

$$\gamma H \ll 1. \tag{36}$$

This is an additional restriction on the validity of the quasi-stationary thin-front limit (32)–(34); not only must the system satisfy the condition $H \gg 1$, but γ must be sufficiently small that $\gamma H \ll 1$. Otherwise the time derivatives in equations (22) and (23) cannot be neglected.

4. Thin-Front Asymptotics

In section 3 we showed how the thin-front limit can be obtained from the reactive-transport equations (22)–(24) by a double limiting process $\gamma \to 0$ and $H \to \infty$. The condition $\gamma H \ll 1$ must also be satisfied to eliminate the time-dependent term in equation (32) (Appendix A). Here we endeavor to explain the hidden assumptions in *Chadam et al.* [1986], and why their conclusion that $\gamma \to 0$ is a sufficient condition for a thin front is incorrect.

Chadam et al. [1986] introduced a time scale (t^* in their notation), which apart from numerical constants is equivalent to the mineral dissolution time t_d. Next they scaled length by $(Dt_d)^{1/2}$ and time by $\gamma^{-1}t_d$

$$\hat{\boldsymbol{r}} = \frac{\boldsymbol{r}}{(Dt_d)^{1/2}}, \quad \hat{t} = \frac{\gamma t}{t_d}, \quad \hat{\boldsymbol{v}} = \boldsymbol{v}\sqrt{\frac{t_d}{D}}, \tag{37}$$

where a hat is used to identify variables with the new scaling. Then, from (1)–(3) the following dimensionless equations are obtained [*Chadam et al.*, 1986]

$$\gamma \hat{\partial}_t \phi + \hat{\nabla} \cdot \hat{\boldsymbol{v}} = 0, \tag{38}$$

$$\gamma \hat{\partial}_t (\phi \tilde{c}) + \hat{\nabla} \cdot (\hat{\boldsymbol{v}} \tilde{c}) = \hat{\nabla}^2 \tilde{c} - \hat{\partial}_t \phi, \tag{39}$$

$$\gamma \hat{\partial}_t \phi = \tilde{c}\, \Theta(\phi_1 - \phi), \tag{40}$$

where equation (40) was used to replace the reaction term in (39) with $\hat{\partial}_t \phi$.

Equations (38)–(40) are equivalent to (22)–(24) when $\gamma > 0$. However, in taking the limit $\gamma \to 0$ we must ensure that there are no hidden powers of γ in the derivatives of the fields. For example, in equation (40) it appears that the left hand side is of order γ, suggesting it can be neglected in the limit $\gamma \to 0$. But this is not true, because the choice of time scale (37) makes the derivative $\hat{\partial}_t \phi$ of order γ^{-1} and the left-hand side of order one overall, as in equation (31). Thus the conclusion in *Chadam et al.* [1986] that the left-hand side of (40) vanishes as $\gamma \to 0$ is incorrect in the general case.

The $\gamma \to 0$ limit in equation (40) only exists if we impose the additional condition that t_d is held constant. Then $\hat{\partial}_t \phi$ is order one and the left-hand side of (40) vanishes when $\gamma = 0$. But, if $t_d = (ks\gamma)^{-1}$ is to be constant, then the reaction rate must diverge as $\gamma \to 0$; in nondimensional terms, H must diverge as $\gamma \to 0$ so as to keep the product γH fixed. Thus, the derivation in *Chadam et al.* [1986] is not inconsistent with section 3, but it is precisely the special case of a fast reaction limit (32)–(34). It is a less general condition than the small γ limit implied by (29)–(31), and a significant portion of the parameter space ($H \lesssim 1$) has been lost.

5. Interface Stability in the Thin-Front Limit

The reaction-infiltration equations (26–31) permit stationary one-dimensional solutions in a frame $x' = x - Ut$, moving with velocity U. In the thin-front limit ($H \gg 1$) the porosity has a jump discontinuity at $x' = 0$: $\phi(x' < 0) = \phi_1$, and $\phi(x' > 0) = \phi_0$. The upstream concentration field is, from (14),

$$\tilde{c} = 1 - \exp(\tilde{x}') \quad \tilde{x}' < 0, \tag{41}$$

while downstream ($\tilde{x}' > 0$) the concentration vanishes. A balance between the incoming flux of reactant, $(v_0 - U)c_{in}$, and its consumption at the front, $U(\phi_1 - \phi_0)c_{sol}$, gives the front velocity

$$U = \frac{\gamma v_0}{(\phi_1 - \phi_0)(1+\gamma)}, \tag{42}$$

which in the limit $\gamma \to 0$ is simply

$$U=\frac{\gamma v_0}{\phi_1-\phi_0}. \tag{43}$$

In the same limit, the fluid velocity in the comoving frame is independent of the front speed.

Chadam et al. [1986] and *Ortoleva et al.* [1987b] derived a dispersion relation describing the growth rate (ω) of small perturbations to a planar dissolution front, but valid only when $H \gg 1$ (section 4). In our notation the result from *Ortoleva et al.* [1987b] is

$$\tilde{\omega}=\frac{1}{1+\Gamma}\left(1+(1-\Gamma)\tilde{u}-\sqrt{1+4\tilde{u}^2}\right), \tag{44}$$

where $u=2\pi/\lambda$ is the wave number of the perturbation and $\Gamma=K_0/K_1$ is the permeability contrast. The dimensionless quantities are (Appendix B): $\tilde{\omega}=\omega l_t/U$ and $\tilde{u}=ul_t$ ($l_t=D/v_0$). Importantly, the interface is only unstable to long wavelength perturbations $u < u_{\text{lim}}$, with a limiting wave number [*Chadam et al.*, 1986]

$$\tilde{u}_{\text{lim}}=\frac{2(1-\Gamma)}{3+2\Gamma-\Gamma^2}. \tag{45}$$

If the width of the system (W) is less than π/u_{lim}, then the longest wavelength in the system ($\lambda_{\text{lim}}=2W$) is stable and the front remains flat. By contrast, in the convection-dominated limit ($H \to 0$) all wavelengths are unstable [*Szymczak and Ladd*, 2013].

A new criterion for an unstable front was proposed in *Zhao et al.* [2013b] and *Zhao* [2014, chap. 11],

$$Zh > \frac{3+2\Gamma-\Gamma^2}{2(1-\Gamma)}\hat{u}, \tag{46}$$

where $Zh=v_0/\sqrt{Dks\gamma}$ is a dimensionless group. Because Zh contains the reaction rate, it has been claimed that this is a more general stability condition than (45), valid for a range of reaction rates [*Zhao et al.*, 2013b; *Zhao*, 2014; *Lai et al.*, 2016]. However, because it follows the same scaling, it is actually identical to the stability criterion in *Ortoleva et al.* [1987b]. Although the connection is hidden in the scaling, by noting that

$$\hat{u}=u\sqrt{Dt_d}=\frac{\tilde{u}v_0}{D}\sqrt{D/ks\gamma}=\tilde{u}Zh, \tag{47}$$

it can be seen that equation (46) is identical to (45). We would also point out that attempts to extend this expression to cases where γ is not vanishingly small [*Zhao et al.*, 2013b] fail, because the condition for a quasi-stationary transport equation, $\gamma H \ll 1$, is violated.

6. Conclusions

In this paper we have offered a critical review of the reaction-infiltration instability, pointing out two significant misconceptions that have arisen from hidden assumptions in the asymptotic analysis. First, that the mineral dissolution ratio (γ) plays a role in determining the degree of reactant penetration; second, that in the limit $\gamma \to 0$ the reactant concentration downstream of the front vanishes [*Chadam et al.*, 1986; *Ortoleva et al.*, 1987a; *Chadam et al.*, 1988; *Chadam and Ortoleva*, 1990; *Zhao et al.*, 2008, 2010, 2013a, 2014; *Zhao*, 2014; *Zhao et al.*, 2015]. Both these statements are incorrect. Equations (27) and (30) show that the mineral dissolution ratio (γ) plays no role in determining the quasi-stationary concentration profile; in particular, the downstream concentration only vanishes when $H \gg 1$.

We have further shown that the thin-front or Stefan limit, first derived in *Chadam et al.* [1986], is actually a double limit, requiring both $\gamma \to 0$ and $H \gg 1$. The condition $\gamma \to 0$ is necessary for a steady state to be achieved without significant mineral dissolution, while the condition $H \gg 1$ ensures that the interface separating dissolved and undissolved mineral remains sharp. Results from Appendix A suggest a general criterion for the quasi-steady approximation is $\max(\gamma, \gamma H) < 0.1$. When dissolution is reaction limited ($H < 1$), the condition is almost always satisfied. However, in the case of transport-limited dissolution ($H \gg 1$), the condition is more stringent. The range of infiltration velocities that can be described by the thin-front limit is bounded from above by the condition $H > 1$ and from below by $\gamma H < 0.1$. For example, a typical mineral dissolution ratio for calcite is of the order of 10^{-4}, which bounds H in the range $1 < H < 1000$. Assuming a reaction rate constant $k=2\times10^{-5}$ cm/s [*Dreybrodt*, 1996] and a reactive surface area $s = 50$/cm [*Noiriel et al.*,

2009], this puts the velocities for which a thin-front limit is appropriate in the range 10^{-4} cm/s to 3×10^{-6} cm/s.

Attempts to extend the thin-front stability analysis to finite reaction rates [*Zhao et al.*, 2007, 2008, 2010, 2013b] do not lead to new results (see section 5), but only repeat previous calculations [*Chadam et al.*, 1986; *Ortoleva et al.*, 1987a] in a different scaling (47). A stability analysis for a finite-width front ($H\lesssim1$) is possible [*Szymczak and Ladd*, 2014], but closed form solutions can only be obtained for small permeability contrasts ($\Gamma\approx1$).

Appendix A: Time Evolution of the One-Dimensional Transport Equations

In this appendix we investigate the approach of the reactant transport equation (2) to steady state. The goal is to determine under what conditions the mineral dissolution time t_d is the longest time scale in the system. We consider a one-dimensional system on time scales less than t_d so that variations in porosity can be ignored,

$$\phi\partial_t c+v_0\partial_x c=D\partial_x^2 c-ksc\Theta(\phi_1-\phi). \tag{A1}$$

For fast reactions ($H>1$), the slowest relaxation is in the upstream region ($x<0$ and $\phi=\phi_1$), with a relaxation time scale D/v_0^2 that is longer than the reaction time scale $(ks)^{-1}$ (19). On the other hand, when $H<1$ the reaction time scale in the downstream region ($x>0$ and $\phi=\phi_0$) is the slowest process.

If $H>1$, we can assume that the evolution of the upstream concentration profile is not significantly affected by the more rapidly relaxing concentration downstream. Thus we consider the upstream region only and seek a solution to the following problem:

$$\bar\partial_t\tilde c+\bar\partial_x\tilde c=\bar\partial_x^2\tilde c, \tag{A2}$$

$$\tilde c(-\infty,t)=1, \tag{A3}$$

$$\tilde c(0,t)=0, \tag{A4}$$

$$\tilde c(x,0)=1. \tag{A5}$$

The scalings $\bar x=xv_0/D$ and $\bar t=tv_0^2/D\phi_1$ were used to make the equations dimensionless. The boundary condition at $x=0$ could be any fixed value without affecting the relaxation time of the profile. In reality $\tilde c(0,t)$ is time-dependent, but, as $H\to\infty$, $\tilde c(0,t)\to0$ for all times.

The solution can be expressed in terms of complementary error functions [*Bear*, 1988],

$$c(\bar x,\bar t)=1-\frac{1}{2}\left[\mathrm{erfc}\left(\frac{-\bar x+\bar t}{2\bar t^{1/2}}\right)+\exp(\bar x)\mathrm{erfc}\left(\frac{-\bar x-\bar t}{2\bar t^{1/2}}\right)\right], \tag{A6}$$

where $\bar x<0$. At sufficiently long times the argument $-\bar x-\bar t$ is always negative, and we can rewrite the solution as the stationary term plus a time-dependent correction,

$$c(\bar x,\bar t)=1-\exp(\bar x)-\frac{1}{2}\left[\mathrm{erfc}\left(\frac{-\bar x+\bar t}{2\bar t^{1/2}}\right)-\exp(\bar x)\mathrm{erfc}\left(\frac{\bar x+\bar t}{2\bar t^{1/2}}\right)\right]. \tag{A7}$$

Since the arguments of both complementary error functions are now positive (assuming $\bar t>\bar x$), we can determine the leading order correction from the asymptotic expansion of $\mathrm{erfc}(x)$,

$$c(\bar x,\bar t)=1-\exp(\bar x)-\frac{2\bar x\bar t^{1/2}}{\pi^{1/2}(\bar t^2-\bar x^2)}\exp\left(\frac{-(\bar t-\bar x)^2}{4\bar t}\right).$$

The time-dependent solution converges to the steady state as $\exp(-\bar t/4)$. Numerically we find the corrections in the domain $\bar x<0$ are small when $\bar t>10$. When $\bar t=10$, the largest deviations, found near $\bar x\sim-1$, are less than 0.1%; by $\bar t=100$ they are negligible ($\approx10^{-14}$). For an accuracy of 0.1%, the criterion for the quasi steady state approximation to be valid is $t_d=(ks\gamma)^{-1}>10D/v_0^2$ (taking $\phi_1=1$). Dissolution under conditions where $H>1$ and $\gamma H<0.1$ can therefore be treated by a quasi-steady approximation.

If $H<1$, we ignore the relaxation of the upstream concentration, and seek a solution to the downstream problem,

$$\bar{\partial}_{\bar{t}}\tilde{c}+\bar{v}\bar{\partial}_{\bar{x}}\tilde{c}=\bar{\partial}_{\bar{x}}^2\tilde{c}-\tilde{c}, \tag{A8}$$

$$\tilde{c}(0,\bar{t})=1, \tag{A9}$$

$$\tilde{c}(\infty,\bar{t})=0, \tag{A10}$$

$$\tilde{c}(\bar{x},0)=0. \tag{A11}$$

The scalings $\bar{x}=x/\sqrt{Dt_r}$, $\bar{t}=t/t_r\phi_0$, and $\bar{v}=v_0/\sqrt{D/t_r}=H^{-1/2}$ were used to make the equations dimensionless. The approximate boundary condition $\tilde{c}(0,\bar{t})=1$ becomes exact in the limit $H\rightarrow 0$. The solution can again be expressed in terms of complementary error functions [*Bear*, 1988],

$$c(\bar{x},\bar{t})=\frac{1}{2}\left[\exp\left(\frac{\bar{x}(\bar{v}-\bar{u})}{2}\right)\mathrm{erfc}\left(\frac{\bar{x}-\bar{u}\bar{t}}{2\bar{t}^{1/2}}\right)+\exp\left(\frac{\bar{x}(\bar{v}+\bar{u})}{2}\right)\mathrm{erfc}\left(\frac{\bar{x}+\bar{u}\bar{t}}{2\bar{t}^{1/2}}\right)\right], \tag{A12}$$

where $\bar{u}=\sqrt{\bar{v}^2+4}$. Once again we can extract the stationary solution, together with a correction term valid for large $\bar{t}$,

$$c(\bar{x},\bar{t})=\exp\left(\frac{-\bar{x}(\bar{u}-\bar{v})}{2}\right)-\frac{2\bar{t}^{1/2}\bar{x}}{\pi^{1/2}(\bar{u}^2\bar{t}^2-\bar{x}^2)}\exp\left(-\frac{\bar{u}^2\bar{t}^2-2\bar{v}\bar{t}\bar{x}+\bar{x}^2}{4\bar{t}}\right). \tag{A13}$$

The asymptotic decay to steady state is now dependent on H as well as $\bar{x}$. The largest deviations from steady state occur around $\bar{x}=\bar{v}\bar{t}$; these terms vanish as $\exp(-\bar{t})$. Numerical calculations again confirm this dependence on $\bar{t}$, with $\bar{t}>7$ for 0.1% accuracy. In other words, for $H<1$ the quasi steady state approximation will hold (within 0.1%) whenever $\gamma<0.15$.

Appendix B: Instability in the Thin-Front Limit

In the thin-front limit ($H\gg 1$), the system can be divided into an upstream region where all the soluble material is dissolved ($\phi=\phi_1$) and a downstream region where the material remains completely undissolved ($\phi=\phi_0$). The boundary between these two regions is sharp and can be described by a curve $\boldsymbol{r}_f(t)$; all the dissolution takes place in an infinitesimal region located along this curve and the problem is to determine the time evolution of $\boldsymbol{r}_f$. Here we determine the development of small perturbations from an initially planar front.

A planar front propagates with a steady velocity U (43) and we define a coordinate system $x'=x-Ut$ moving with this mean front position. For small perturbations we can parameterize the local front position relative to the mean as a function of y,

$$x_f'(y)=\delta\exp(\omega t)\cos(uy), \tag{B1}$$

where δ is the amplitude of the perturbation. In the linear regime it is sufficient to treat the perturbations as individual Fourier modes, characterized by a wavelength $\lambda=2\pi/u$ and an amplitude δ. The growth (or decay) of each individual mode is determined by $\omega(u)$.

For a planar front the pressure is a linear function of position, $p=-\alpha x'$, where $\alpha=\mu v_0/K(\phi)$ and the pressure is set to zero at the front. The pressure gradient is different in the two regions because of the variation in permeability, but both the pressure and velocity are continuous at the front. Next we calculate the change in the pressure field when the front is perturbed according to equation (B1). We will write the solutions separately in each region and then match them at the front.

$$p_1=-\alpha_1 x'+\delta_{p_1}\exp(ux')\exp(\omega t)\cos(uy)\quad x'<x_f', \tag{B2}$$

$$p_0=-\alpha_0 x'+\delta_{p_0}\exp(-ux')\exp(\omega t)\cos(uy)\quad x'>x_f'. \tag{B3}$$

The perturbations satisfy the Laplace equation $\nabla^2 p=0$ in their respective domains, and vanish far from the front. They contain the same Fourier component as the front perturbation in order to satisfy the boundary conditions.

The matching condition, $p_1(x_f')=p_0(x_f')$, requires care because the front is not located exactly at $x'=0$, but within a linear approximation

$$p(x_f')=p(0)+x_f'(\partial_{x'}p)_{x'=0}. \tag{B4}$$

Combining equations (B2)–(B4) with the matching condition on the pressure, we have (to linear order in the perturbations)

$$-\alpha_1\delta+\delta_{p_1}=-\alpha_0\delta+\delta_{p_0}. \tag{B5}$$

Continuity of mass across the interface requires matching the normal pressure gradients as well,

$$K_1(\boldsymbol{n}\cdot\nabla p_1)_{x'=x_f'}=K_0(\boldsymbol{n}\cdot\nabla p_0)_{x'=x_f'}. \tag{B6}$$

For small perturbations, the location of the boundary has no effect on the pressure gradient

$$(\nabla p)_{x'=x_f'}=-\alpha\boldsymbol{e}_x+u\delta_p\exp(\omega t)\left[\pm\cos(uy)\boldsymbol{e}_x-\sin(uy)\boldsymbol{e}_y\right], \tag{B7}$$

where the remaining contributions are of order δ^2 and beyond. The surface-normal points predominantly in the x direction

$$\boldsymbol{n}=\boldsymbol{e}_x-\delta\sin(uy)\boldsymbol{e}_y, \tag{B8}$$

and the matching condition to linear order is

$$K_1\delta_{p_1}=-K_0\delta_{p_0}. \tag{B9}$$

Combining (B5) and (B9), we can solve for the coefficients δ_p in terms of the amplitude of the front perturbation δ

$$\delta_{p_1}=-\frac{\mu v_0}{K_1}\frac{1-\Gamma}{1+\Gamma}\delta,\quad \delta_{p_0}=\frac{\mu v_0}{K_0}\frac{1-\Gamma}{1+\Gamma}\delta, \tag{B10}$$

as before, $\Gamma=K_0/K_1$ is the permeability contrast. These expressions can be further simplified by introducing the constant $\beta=(1-\Gamma)/(1+\Gamma)$

$$\delta_{p_1}=-\alpha_1\beta\delta,\quad \delta_{p_0}=\alpha_0\beta\delta. \tag{B11}$$

The concentration field in the upstream region $c_1(x',y)$ is the solution of the convection-diffusion equation (27), with boundary conditions $c_1(-\infty,y)=c_{in}$ and $c_1(x_f'(y),y)=0$. Combining the solution for a planar front (14) with a term describing a single Fourier mode perturbation,

$$c_1=c_{in}[1-\exp(x'v_0/D)+\delta_c(x')\exp(\omega t)\cos(uy)]; \tag{B12}$$

in this case the amplitude of the perturbation $\delta_c(x')$ is a function we need to solve for. The fluid velocity, $\boldsymbol{v}_1=-K_1\nabla p_1/\mu$, can be determined from equations (B2) and (B11),

$$\boldsymbol{v}_1=v_0\left[\boldsymbol{e}_x+\beta u\delta\exp(\omega t+ux')\{\cos(uy)\boldsymbol{e}_x-\sin(uy)\boldsymbol{e}_y\}\right]. \tag{B13}$$

Combining (B12) and (B13) with the convection-diffusion equation $v_1\cdot\nabla c=D\nabla^2 c$ results in an equation for $\delta_c(x')$

$$l_t^2\partial_x^2\delta_c-l_t\partial_x\delta_c-(ul_t)^2\delta_c=-\beta u\delta\exp(ux'+x'/l_t), \tag{B14}$$

where $l_t=D/v_0$ is the transport length scale. The solution of (B14) is

$$\delta_c(x')=C_+\exp(\lambda_+x'/l_t)+C_-\exp(\lambda_-x'/l_t)-\beta\delta l_t^{-1}\exp[(u+l_t^{-1})x'], \tag{B15}$$

where the coefficients $C_\pm$ are determined by the boundary conditions at $-\infty$ and x_f'. The exponents $\lambda_\pm=(1\pm\sqrt{1+4(ul_t)^2})/2$ are the roots of the characteristic equation.

The perturbations in concentration must die out far from the front ($x'\to-\infty$), implying that $C_-=0$. The boundary condition at the front $c_1(x_f'(y),y)=0$ is, to linear order in the perturbations,

$$-\frac{\delta}{l_t}+C_+-\frac{\delta\beta}{l_t}=0. \tag{B16}$$

The solution for the concentration perturbation is then

$$\delta_c(x')=\frac{\delta}{l_t}[(1+\beta)\exp(\lambda_+x'/l_t)-\beta\exp((1+ul_t)x'/l_t)]. \tag{B17}$$

The reactant flux $\boldsymbol{J}(x_f'(y),y)$ at the boundary is purely diffusive (since $c_1(x_f'(y),y)=0$),

$$\boldsymbol{J}=-D(\boldsymbol{nn}\cdot\nabla c_1)_{x'=x_f'}. \tag{B18}$$

At linear order, only the x derivative makes a contribution to the flux (B8), while the perturbation can again be calculated at the mean position $x'=0$

$$J_x=-Dc_{in}\left[-\frac{1}{l_t}-\frac{x_f'}{l_t^2}+(\partial_{x'}\delta_c)_{x'=0}\exp(\omega t)\cos(uy)\right]. \tag{B19}$$

The flux contains the contribution from the planar front v_0c_{in} in addition to the perturbations.

When the front advances by a small increment dx_f, it consumes an amount of mineral (per unit area) $dM=(\phi_1-\phi_0)c_{sol}dx_f=J_xdt$. The front then advances with a local velocity

$$\frac{dx_f}{dt}=\frac{v_0c_{in}}{(\phi_1-\phi_0)c_{sol}}\left[1+\frac{\delta}{l_t}\exp(\omega t)\cos(uy)[1-(1+\beta)\lambda_++\beta(1+ul_t)]\right]. \tag{B20}$$

Thus, a planar front ($\delta=0$) propagates with a velocity U, given by equation (43), while perturbations in the front grow (or decay) exponentially $dx_f'/dt=\omega x_f'$, at a rate

$$\omega=\frac{U}{l_t}\left[1+\beta(1+ul_t)-(1+\beta)\frac{1+\sqrt{1+4(ul_t)^2}}{2}\right]. \tag{B21}$$

The characteristic time scale for the growth of perturbations in the thin-front limit is then l_t/U. After some rearrangement of equation (B21), we obtain the result quoted in equation (44), replacing ul_t by the dimensionless wave number $\tilde{u}$ and $\omega l_t/U$ by $\tilde{\omega}$,

Acknowledgments

Anthony J. C. Ladd acknowledges the support of the U.S. Department of Energy Office of Science, Office of Basic Energy Sciences under award DEFG02-98ER14853. Piotr Szymczak acknowledges support from the SHALESEQ project (Physicochemical effects of CO2 sequestration in the Pomeranian gas bearing shales), funded by the Polish-Norwegian Research Programme operated by the National Centre for Research and Development under the Norwegian Financial Mechanism 2009-2014 (project contract no. POL-NOR/234198/100/2014). The paper contains no externally generated data.

References

Bear, J. (1988), *Dynamics of Fluids in Porous Media*, Dover, New York.

Chadam, D., D. Hoff, E. Merino, P. Ortoleva, and A. Sen (1986), Reactive infiltration instabilities, *J. Appl. Math.*, *36*, 207–221.

Chadam, D., P. Ortoleva, and A. Sen (1988), A weakly nonlinear stability analysis of the reactive infiltration interface, *SIAM J. Appl. Math.*, *48*, 1362–1378.

Chadam, J., and P. Ortoleva (1990), Morphological instabilities in physico-chemical systems, *Earth Sci. Rev.*, *29*, 175–181.

Chadam, J., P. Ortoleva, Y. Qin, and R. Stamicar (2001), The effect of hydrodynamic dispersion on reactive flows in porous media, *Eur. J. Appl. Math.*, *12*, 557–569.

Daccord, G. (1987), Chemical dissolution of a porous medium by a reactive fluid, *Phys. Rev. Lett.*, *58*(5), 479–482.

Detwiler, R. (2010), Permeability alteration due to mineral dissolution in partially saturated fractures, *J. Geophys. Res.*, *115*, B09210, doi: 10.1029/2009JB007206.

Detwiler, R. L., R. J. Glass, and W. L. Bourcier (2003), Experimental observations of fracture dissolution: The role of Péclet number in evolving aperture variability, *Geophys. Res. Lett.*, *30*(12), 1648, doi:10.1029/2003GL017396.

Dreybrodt, W. (1996), Principles of early development of karst conduits under natural and man-made conditions revealed by mathematical analysis of numerical models, *Water Resour. Res.*, *32*, 2923–2935.

Ewers, R. O. (1982), Cavern development in the dimensions of length and breadth, PhD thesis, McMaster Univ., Hamilton, Ont., Canada.

Fredd, C. N., and H. S. Fogler (1998), Influence of transport and reaction on wormhole formation in porous media, *AIChE J.*, *44*, 1933–1949.

Golfier, F., M. Quintard, and S. Whitaker (2002), Heat and mas transfer in tubes: An analysis using the method of volume averaging, *J. Porous Media*, *5*, 169–185.

Hinch, E. J., and B. S. Bhatt (1990), Stability of an acid front moving through porous rock, *J. Fluid Mech.*, *212*, 279–288.

Hoefner, M. L., and H. S. Fogler (1988), Pore evolution and channel formation during flow and reaction in porous media, *AIChE J.*, *34*, 45–54.

Kelemen, P., J. Whitehead, E. Aharonov, and K. Jordahl (1995), Experiments on flow focusing in soluble porous media, with applications to melt extraction from the mantle, *J. Geophys. Res.*, *100*, 475–496.

Lai, K.-H., J.-S. Chen, C.-W. Liu, S.-Y. Shu, and C. Steefel (2016), Effect of medium permeability anisotropy on the morphological evolution of two non-uniformities in a geochemical dissolution system, *J. Hydrol.*, *533*, 224–233, doi:10.1016/j.jhydrol.2015.11.039.

Lichtner, P. C. (1988), The quasi-stationary state approximation to coupled mass transport and fluid-rock interaction in a porous media, *Geochim. Cosmochim. Acta*, *52*, 143–165.

Luquot, L., and P. Gouze (2009), Experimental determination of porosity and permeability changes induced by injection of CO_2 into carbonate rocks, *Chem. Geol.*, *265*(1–2), 148–159, doi:10.1016/j.chemgeo.2009.03.028.

Luquot, L., O. Rodriguez, and P. Gouze (2014), Experimental characterization of porosity structure and transport property changes in limestone undergoing different dissolution regimes, *Transp. Porous Media*, *101*(3), 507–532.
Noiriel, C., L. Luquot, B. Madé, L. Raimbault, P. Gouze, and J. van der Lee (2009), Changes in reactive surface area during limestone dissolution: An experimental and modelling study, *Chem. Geol.*, *265*, 160–170.
Noiriel, C., P. Gouze, and B. Made (2013), 3D analysis of geometry and flow changes in a limestone fracture during dissolution, *J. Hydrol.*, *486*, 211–223.
Ortoleva, P., J. Chadam, E. Merino, and A. Sen (1987a), Geochemical self-organization II: The reactive-infiltration instability, *Am. J. Sci.*, *287*, 1008–1040.
Ortoleva, P., E. Merino, C. Moore, and J. Chadam (1987b), Geochemical self-organization I: Reaction-transport feedbacks and modeling approach, *Am. J. Sci.*, *287*(10), 979–1007.
Osselin, F., A. Budek, O. Cybulski, P. Kondratiuk, P. Garstecki, and P. Szymczak (2016), Microfluidic observation of the onset of reactive infiltration instability in an analog fracture, *Geophys. Res. Lett.*, *43*, 6907–6915.
Phillips, O. M. (1990), Flow-controlled reactions in rock fabrics, *J. Fluid Mech.*, *212*, 263–278.
Plummer, L. N., and T. L. M. Wigley (1976), The kinetics of calcite dissolution in CO_2-water systems at 25°C and 1 atmosphere total pressure, *Geochim. Cosmochem. Acta*, *40*, 191–202.
Polak, A., D. Elsworth, J. Liu, and A. S. Grader (2004), Spontaneous switching of permeability changes in a limestone fracture with net dissolution, *Water Resour. Res.*, *40*, W03502, doi:10.1029/2003WR002717.
Rowan, G. (1959), Theory of acid treatment of limestone formations, *J. Inst. Pet.*, *45*(431), 321.
Steefel, C. I., and A. C. Lasaga (1990), Evolution of dissolution patterns: Permeability change due to coupled flow and reaction, in *Chemical Modeling of Aqueous Systems II*, edited by D. C. Melchior and R. L. Bassett, pp. 212–225, Am. Chem. Soc., Washington, D. C.
Szymczak, P., and A. J. C. Ladd (2012), Reactive infiltration instabilities in rocks. Fracture dissolution, *J. Fluid Mech.*, *702*, 239–264.
Szymczak, P., and A. J. C. Ladd (2013), Interacting length scales in the reactive-infiltration instability, *Geophys. Res. Lett.*, *40*, 3036–3041, doi:10.1002/grl.50564.
Szymczak, P., and A. J. C. Ladd (2014), Reactive infiltration instabilities in rocks. Part 2. Dissolution of a porous matrix, *J. Fluid Mech.*, *738*, 591–630.
Wangen, M. (2013), Stability of reaction-fronts in porous media, *Appl. Math. Modell.*, *37*, 4860–4873, doi:10.1016/j.apm.2012.10.004.
Zhao, C. (2014), *Physical and Chemical Dissolution Front Instability in Porous Media: Theoretical Analyses and Computational Simulations*, Springer, Cham.
Zhao, C., B. E. Hobbs, A. Ord, P. Hornby, and S. Peng (2007), Effect of reactive surface areas associated with different particle shapes on chemical-dissolution front instability in fluid-saturated porous rocks, *Transp. Porous Media*, *73*(1), 75–94, doi:10.1007/s11242-007-9162-z.
Zhao, C., B. E. Hobbs, P. Hornby, A. Ord, S. Peng, and L. Liu (2008), Theoretical and numerical analyses of chemical-dissolution front instability in fluid-saturated porous rocks, *Int. J. Numer. Anal. Methods Geomech.*, *32*(9), 1107–1130, doi:10.1002/nag.661.
Zhao, C., B. Hobbs, A. Ord, and S. Peng (2010), Effects of mineral dissolution ratios on chemical-dissolution front instability in fluid-saturated porous media, *Transp. Porous Media*, *82*(2), 317–335, doi:10.1007/s11242-009-9427-9.
Zhao, C., T. Poulet, K. Regenauer-Lieb, and B. Hobbs (2013a), Computational modeling of moving interfaces between fluid and porous medium domains, *Comput. Geosci.*, *17*, 151–166, doi:10.1007/s10596-012-9322-2.
Zhao, C., B. E. Hobbs, and A. Ord (2013b), Theoretical analyses of acidization dissolution front instability in fluid-saturated carbonate rocks, *Int. J. Numer. Anal. Methods Geomech.*, *37*(13), 2084–2105, doi:10.1002/nag.2123.
Zhao, C., B. E. Hobbs, and A. Ord (2014), Theoretical analyses of acidization dissolution front instability in fluid-saturated porous media under non-isothermal conditions, *Int. J. Numer. Anal. Methods Geomech.*, *39*(13), 799–820, doi:10.1002/nag.2123.
Zhao, C., B. E. Hobbs, and A. Ord (2015), Computational simulation of chemical dissolution-front instability in fluid-saturated porous media under non-isothermal conditions, *Int. J. Numer. Methods Eng.*, *102*, 135–156, doi:10.1002/nme.